Calculation of radioactive isotope production cross-sections with FLUKA and their application to radiological studies

M. Brugger, A. Ferrari, M. Magistris, S. Roesler, J. Vollaire
CERN, Geneva, Switzerland

Abstract

During the lifetime of a high-energy accelerator estimations of induced radioactivity are important in all its phases, such as design, operation and decommissioning. FLUKA's capability of making predictions for isotope production in hadronic showers has been subject to extensive benchmark experiments carried out in the last years. The accuracy of these predictions steadily improved with the advancements of models implemented into FLUKA, in particular after the introduction of a new evaporation/ fragmentation model and the improvements and extensions of the PEANUT model.

Whereas former activation studies focused on samples of selected materials and representative source spectra typical for high-energy accelerators, this paper gives a more general analysis of calculated isotope production cross-sections and their application to future radiation protection needs. In this paper a general approach is presented how to quantify calculation uncertainties and use pre-calculated cross-sections in order to fold them with expected energy spectra as encountered around accelerators, thus leading to fast and accurate results. The application of this approach is understood to be an indispensable ingredient, for example in order to efficiently calculate radionuclide inventories needed for disposal of radioactive waste towards the final repositories.

Based on a list of materials and radioactive isotopes, possible reaction channels can be derived for a certain application and energy-dependent isotope production cross-sections are calculated and compared to experimental data. Depending on the amount and accuracy of the available experimental data sets, as well as the production mechanisms of the radioisotopes, respective uncertainty factors can be derived. These factors mainly depend on the production mechanism and the energy range of interest, thus allow quantifying uncertainties in isotope production as calculated with FLUKA in a more global way. Pre-calculated isotope production cross-sections can then be used to estimate radionuclide inventories by folding the cross-sections with expected particle energy spectra. Typical spectra as encountered in high-loss regions of the LHC accelerator are shown and compared to those used in previous benchmark experiments.

Introduction

All stages in the life-cycle of a high energy accelerator require calculations of induced radioactivity. During the construction phase their results enter the design of components and the choice of materials, during operation they provide dose estimates for work on activated components and also the de-commissioning of an accelerator is based on studies of the nuclide inventory. For accelerators reaching TeV energies, a Monte Carlo code used for such calculations must be able to reliably predict nuclide production in interactions of all stable hadrons on arbitrary target elements and at energies ranging from that of thermal neutrons to several TeV. For this reason, most studies for the Large Hadron Collider (LHC) employ FLUKA [1,2] as it was found to be the most appropriate Monte Carlo code for estimations of induced radioactivity at this accelerator [3].

In principle, induced radioactivity can be calculated directly in the simulation of the particle cascade in the respective components. Radionuclides follow from the last step of an inelastic interaction and different options exist in FLUKA to score them at any location in the geometry. Moreover, the calculation of radioactive built-up and decay has been added recently such that accurate predictions for nuclide production and induced radioactivity can now be obtained from a single FLUKA simulation without further need to post-process the results.

Although being very convenient the latter one-step simulation is not always the most efficient way to achieve results. Examples for such situations include materials of low density, such as air, for which obtaining results with low statistical uncertainty may imply significant CPU-time if nuclides are calculated directly. Similarly, it is not always efficient to re-run the entire simulation if details in the geometry, such as the definition of trace elements in a material composition, or certain aspects in the nuclide production models have changed.

In these situations it is often more appropriate to follow a two-step approach, by calculating particle fluence spectra in the regions of interest and by folding them off-line with pre-computed, energy-dependent nuclide production cross-sections. These cross-sections can be obtained directly from FLUKA by simulating single collisions but can also include experimental information, if available, in the form of evaluated cross-sections. This two-step approach allows more flexibility and efficiency to explore different design options, for example, in studies of air activation, as well as for applications in which precise predictions are not necessarily required, such as for the radiological characterisation of radioactive waste.

The present study aims at building such a data-base of energy-dependent cross-sections. It is based on FLUKA predictions but also includes experimental data to verify calculated values. The most complete compilation of experimental information for our purposes can be found in Ref. [4]. In addition, dedicated benchmark experiments for activation of materials typically used in the construction of the LHC were performed over the past few years and serve as basis for a verification [3,5].

Cross-sections are calculated according to their relevance for radiological studies for the LHC and therefore cover so far reactions of protons, neutrons and charged pions on nuclei with masses up to zinc. Despite this present limitation the number of calculated cross-section data sets is enormous and a detailed comparison to experimental data can only be performed for selected reactions. For all other channels a more automated approach is attempted in which energy-averaged ratios of measured and calculated cross-sections are computed. These ratios are not meant to allow unambiguous conclusions but should give at least an indication on the performance of FLUKA for single reaction channels.

The prediction of the nuclide vector for radioactive waste considerations has been chosen as a first area of application of the new database. In particular, one of the most radioactive parts of the LHC, the collimation region, was selected. Based on an existing, detailed FLUKA geometry [6] of that area particle fluence spectra were calculated for a large number of different locations and were folded off-line with the pre-computed cross-sections for reactions leading to waste-relevant nuclides. As it is shown below, this approach allows an investigation of the sensitivity of the nuclide predictions on the shape of the fluence spectra and a reduction of all computed spectra to a sub-set of so-called characteristic spectra.

Activation benchmark measurements at CERF

In the past years an extensive collection of samples of different materials such as aluminium, copper, stainless steel, iron, titanium, concrete, marble, boron nitride, carbon composite, and demineralised water were irradiated at the CERN-EU High-Energy Reference Field (CERF) facility [7], using the secondary mixed hadron beam from the Super Proton Synchrotron (SPS) accelerator. The facility is installed in one of the secondary beam lines (H6) from the Super Proton Synchrotron (SPS) at CERN. At this facility a cylindrical copper target (7 cm in diameter, 50 cm in length) is intercepting a positively charged hadron beam with a momentum of 120 GeV/c consisting of protons (34.8%), pions (60.7%) and kaons (4.5%).

The copper target is surrounded by a concrete enclosure of 80 cm thickness. The CERF facility serves mainly for detector test and calibration purposes and thus provides instrumentation for accurately recording the beam properties (intensity and profile). As the latter is essential for benchmark experiments, the facility is well suited for studies of induced radioactivity. An air-filled Precision Ionisation Chamber (PIC) at atmospheric pressure, placed in the beam upstream of the copper target, monitors the intensity of the beam.

In the series of benchmark experiments emphasis was put on reducing uncertainties in both measurements and simulations in order to allow for an accurate benchmark of the FLUKA code. This included low-level gamma spectrometry measurements, appropriate treatment of the decay chains of isotopes in the gamma spectrometry and in the simulations, efficiency correction in the spectrometry, as well as detailed simulations of residual nuclei production with low statistical uncertainties. For each sample spectrometry, analyses were performed for several cooling times, which allowed identifying both short- and long-lived isotopes.

Further details concerning the experimental set-up, the beam conditions and the benchmark results can be found in [5,8,9].

Figure 1: Distribution of high [red (dark grey)] and low [yellow (light grey)] loss regions around the LHC

The two beam cleaning insertions (Points 3 and 7), the dump caverns and the inner triplets will be especially regions of elevated activation

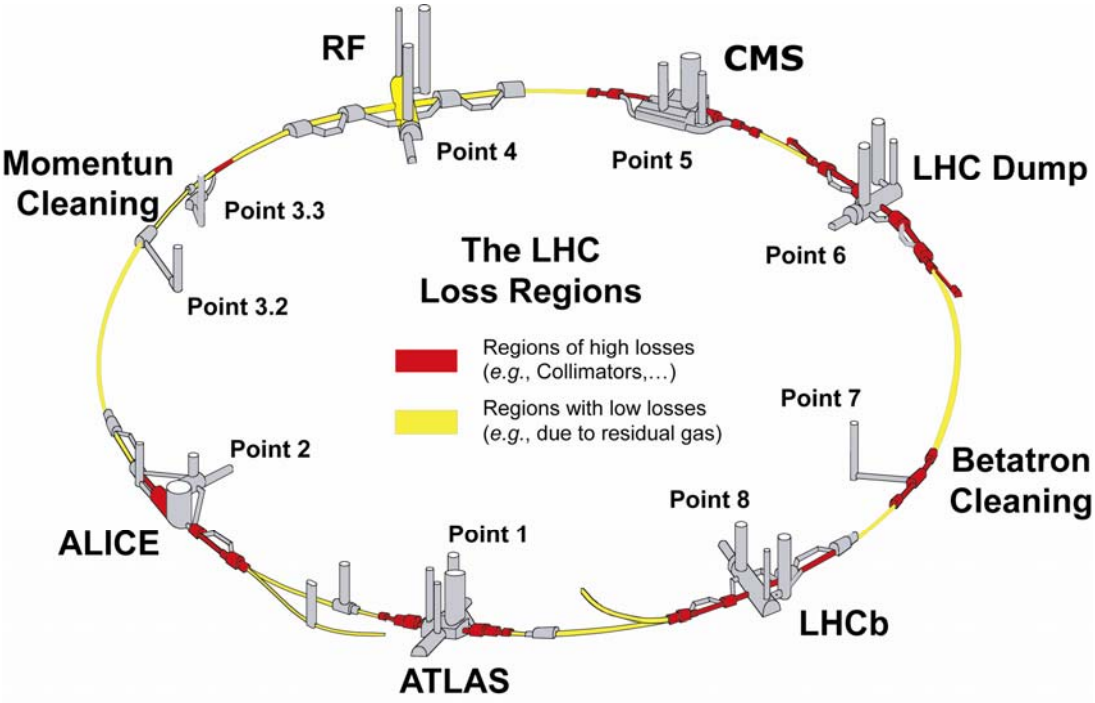

The collimation regions of the LHC

The LHC is a synchrotron-collider which accelerates and stores two intense beams of particles circulating in opposite directions. Its size and structure was given by the former LEP ring which consisted of eight so-called arcs with a bending radius close to 3.5 km linked together by eight 528 m long straight sections. The two beams of the LHC will be accelerated in two separate vacuum chambers side by side in the horizontal plane through the arcs and will cross over at dedicated interaction points (IP) in the centre of those straight sections dedicated to experiments. The high stored total energy and total beam current make the LHC not only a challenging project with respect to its construction, but also to the operation and protection of the accelerator itself.

High energy particle cascades induced by beam particle losses lead to the activation of material in the respective zone of the accelerator. At the LHC one can distinguish machine zones of high and low losses as shown in Figure 1.

The LHC requires numerous different elements in order to assure its stable operation, one of them being the beam cleaning or collimation system. During the high-energy collisions in the physics experiments, particles scattered elastically are emitted in the primary beam direction with the same momentum and a slight increase in transverse angle. The same effect occurs along the whole machine due to elastic interactions between the protons and the residual gas nuclei in the vacuum chamber. Furthermore, beam instabilities (non-linear beam dynamics) also contribute to an amplitude increase of the transverse and longitudinal beam distribution. All these effects will progressively push particles outside of the stable region, creating a so-called beam halo.

One of the challenging tasks in the design of the LHC is the need to ensure this halo to be intercepted at dedicated elements before it hits other parts of the accelerator, *e.g.* the cold inner part of a super-conducting magnet. Already a few per mile of the scattered particle flux interacting with a superconducting magnet would cause it to quench. Therefore, an efficient collimation system is required in order to ensure stable operation of the machine. For this purpose, the LHC includes two cleaning insertions, defined as those parts of the accelerator ring where particle losses are concentrated. One of which is dedicated to clean off-momentum particles, whereas the other captures particles outside a defined transverse boundary, requested to be smaller than the aperture of the remaining accelerator components.

The betatron cleaning insertions at IP7, which is showing the highest losses and where a complicated betatron cleaning system will undergo major upgrades within a phased approach of its installation, is in the following chosen as a test case to verify the presented approach of calculating secondary particle spectra and fold them with pre-calculated (or measured) isotope production cross-sections.

The Monte Carlo code FLUKA

In an inelastic reaction of a high-energy hadron with a nucleus, hadrons will be produced, as well as many individual nucleons and some clusters of nucleons will be ejected from the struck nucleus during the various phases of the interaction. Depending on the mass of the remaining fragment(s) with respect to the mass of the original target nucleus the interactions are classified as spallation, deep spallation/fission or multi fragmentation. The residual nucleus will be left in a highly excited state and will most probably be unstable against radioactive decay. It will attempt to reach a stable configuration by a succession of decays of gradually increasing lifetime (possible exceptions might be metastable states). Low-energy neutrons, protons and pions interact with nuclei via resonance interactions, but these processes generally result in the removal of only a few nucleons from the struck nucleus which is left in a near-stable configuration.

The production of radionuclides in FLUKA [1,2] results directly from the description of hadronic interactions. It can therefore be modelled for any incoming hadron, target nucleus and energy. Interactions of low-energy neutrons ($E < 19.6$ MeV) form the only exception, for which pre-tabulated cross-sections are used. If such cross-sections are not available for a certain target element, radionuclides are not generated in interactions on that element by default. For all other reactions, radionuclides follow directly from the last step of the interaction and results are thus influenced by all previous stages.

Hadronic collisions at energies above several GeV are described within the Dual Parton Model (DPM) which includes multiple interactions of the incoming hadron on target nucleons (so-called Gribov-Glauber theory). These high-energy hadron-nucleon interactions are followed by a sophisticated Generalised Intranuclear Cascade (GINC) model. At energies below a few GeV the description of the interaction starts immediately from the GINC model. The GINC terminates as soon as all produced hadrons (except nucleons) are either emitted, absorbed or decayed and all secondaries have reached energies below a few tens of MeV. The pre-fragment then enters the pre-equilibrium stage immediately followed by a detailed description of evaporation and fragmentation [3,10].

The evaporation module in FLUKA includes approximately 600 possible emitted particles and states with mass numbers below A = 25. The fragmentation of light nuclei (A < 18) follows a Fermi break-up model considering about 50000 different combinations with up to six ejectiles. In addition, coalescence processes are treated in detail. The evaporation model has been improved recently, including the introduction of new level-densities and refined Coulomb barriers.

The implementation in FLUKA of nuclear interactions is called PEANUT. At the time of this study, the DPM was not part of PEANUT limiting the energy range for PEANUT to 5 GeV. An independent implementation of the DPM was responsible for the description of interactions at higher energies which, for historical reasons, included also an independent intra-nuclear cascade model, less-sophisticated than that of PEANUT. The boundary between the two implementations at 5 GeV was typically visible as discontinuity in energy-dependent quantities, such as nuclide production cross-sections, but was of no importance for many applications. Very recently, the DPM has been added to PEANUT allowing a coherent description of interactions at all energies. Moreover, quasi-elastic processes are now consistently modelled, such that the discontinuity should disappear in future releases of FLUKA.

As the character of this study is of more general nature these latest improvements in FLUKA have no direct implication on the conclusions and can be easily incorporated by replacing the nuclide production cross-sections.

Precise predictions about radioisotope production are by far the most demanding tasks for nuclear models. More recently, a vast experimental programme aimed at validating code predictions for radionuclide production have been carried out at CERF in view of the challenges posed by the LHC. The comparisons with the calculated results, both for radionuclide production [3] and for residual dose rates [9], have firmly established the reliability of the code and of its associated inventory evolution algorithms. Of course, since the accuracy of particle energy and spatial fluence predictions is always better than of radionuclide production, every time reliable experimental production cross-sections for a given isotope are available for all particles energies of interest, folding the computed fluences with evaluated experimental cross-sections is the most accurate approach.

Calculations of cross-sections and comparison to experimental data

All radionuclide production cross-sections discussed in the following paragraphs were calculated with a non-standard FLUKA routine. It calls directly the inelastic interaction models for a given combination of projectile, target nucleus and energy and allows scoring of individual residual nuclei. It returns the inelastic cross-section as well as individual radionuclide production cross-sections as shown below.

For the application to waste studies at the CERN LHC accelerator, FLUKA cross-sections were calculated according to their relevance for radiological studies for the LHC and cover therefore so far reactions of protons, neutrons and charged pions on nuclei with masses up to zinc. In total 103 isotopes were studied (^{3}H up to ^{72}Zn) produced on 138 different target materials (heavier materials than Zn were considered as target material because of their importance as trace elements). All calculations were performed separately for the type of the projectile (p, n, π+ and π-) as well as for an energy range from 1 MeV to 10 TeV (except for neutrons were the lower limit was set to 19.6 MeV in order to coincide with the boundary below which tabulated values are used).

To verify the contribution of decay chains in case of isotopes up to zinc, in a first step cumulative (including the production term coming from possible decay reactions of mother isotopes) and non-cumulative cross-sections were compared as shown in Table 1. Cumulative yields contain all contributions from mother isotopes decaying via positive or negative beta decay and having a half-life smaller than the one of the respective isotope of concern.

In the example of isotopes being produced by protons on natural copper it can be seen that for the presented study in a first approximation contributions coming from radioactive decay chains are small (5.7% [^{51}Cr] and 8.3% [^{49}V]). Other projectiles and targets result in comparable contributions, thus for the presented study it was decided to use cumulative cross-sections only. For cases were the experimental data are given as non-cumulative only, calculated cumulative and non-cumulative cross-sections were compared to each other and didn't show a difference significant for the presented calculations.

Table 1: Isotopes produced by protons on natural copper showing differences in their calculated values for cumulative and non-cumulative cross-sections

Values are given as average difference (in per cent) of the respective energy-dependent cross-section for the two cases

Isotope	Cummulative Contribution [%]	Isotope	Cummulative Contribution [%]	Isotope	Cummulative Contribution [%]
Al26	0.027	*Cr55*	1.211323927	*Na24*	2.222
Al29	0.268	*Cu60*	0.266004106	*Ne24*	0.593
Ar37	0.110	*Cu61*	0.452601945	*Ni57*	0.013
Ar39	3.076	*F18*	0.122197941	*Ni59*	0.828
Ar41	1.089	*Fe53*	0.020957495	*Ni63*	2.634
Ar42	0.329	*Fe55*	1.833566652	*P33*	0.458
Ar43	0.572	*Fe59*	0.554082518	*S35*	2.091
C14	0.480	*Fe60*	0.089785773	*S37*	0.630
Ca41	0.040	*K43*	0.518175331	*Sc43*	0.106
Ca45	1.917	*K44*	0.647122696	*Sc49*	0.085
Ca47	1.318	*K45*	0.140056222	*Si31*	0.685
Cl34	0.010	*Mg27*	0.707324503	*Si32*	0.182
Cl39	0.227	*Mg28*	0.132847233	*Ti45*	0.017
Cl40	0.082	*Mn51*	0.022365327	*Ti51*	0.408
Co55	0.140	*Mn52*	1.546496611	*V47*	0.024
Co56	0.805	*Mn53*	3.840444367	*V48*	1.159
Co57	2.256	*Mn56*	0.683478807	*V49*	8.325
Co61	0.552	*Mn57*	0.363748906	*V52*	1.137
Cr49	0.028	*N13*	0.666154655	*V53*	0.416
Cr51	5.770	*Na22*	0.014799518	*Zn63*	0.003

Despite the present restrictions in isotopes and target materials typical for LHC applications, the number of calculated cross-section data sets is still enormous; a detailed comparison to experimental data can only be performed for selected reactions. The latter were chosen to be representative cases depending on the mass difference of the remaining fragment with respect to the mass of the original target nucleus, thus classified as spallation, deep spallation or multi-fragmentation and low-energy neutron reactions, their reaction mechanisms, as well as for their importance for studies concerning the radioactive waste at CERN. This allows testing the quality of FLUKA to predict such isotopes in different energy ranges.

The selected cross-sections used for this study are:

- ^{22}Na produced on natural iron;
- ^{60}Co produced on natural copper;
- ^{54}Mn produced on natural iron;
- ^{54}Mn produced on natural manganese;
- ^{154}Eu produced on natural europium;
- ^{54}Mn produced on ^{55}Mn;
- ^{60}Co produced on ^{59}Co.

The respective energy dependent isotope production cross-sections as calculated with FLUKA are shown in Figure 2.

Figure 2: Energy-dependent isotope production cross-sections of the selected representative isotopes

Please note that in the case of ^{60}Co and ^{54}Mn the shown neutron cross-sections are only valid for energies above 19.6 MeV. For energies below tabulated values have to be used as shown for ^{154}Eu (produced on natural europium), ^{60}Co (^{59}Co) or ^{54}Mn (^{55}Mn).

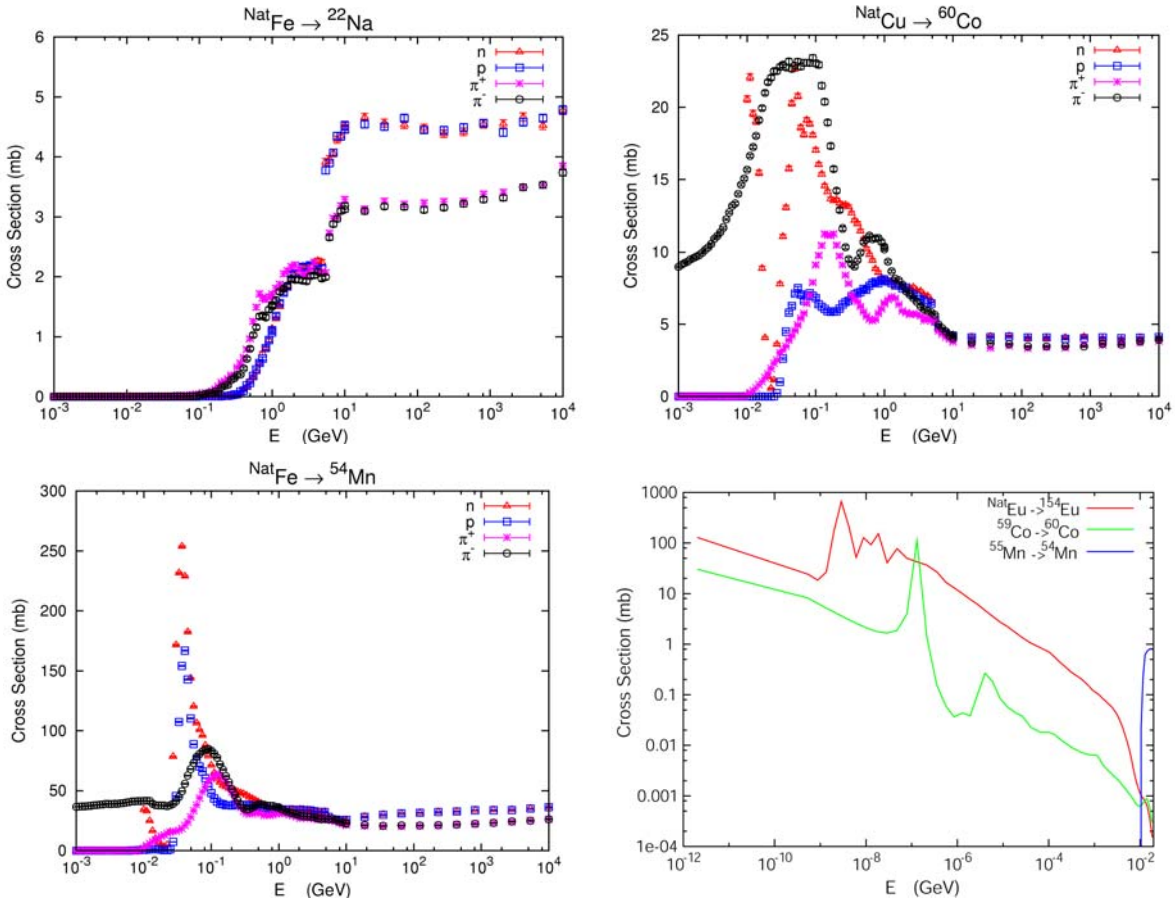

In a first analysis these isotope production cross-sections were compared with published values measured in numerous experiments and collected in the Landolt-Börnstein compendium [4]. It shall be noted that depending on the isotope some of the available experimental data tend to fluctuate significantly as a function of energy, thus for the representative isotopes cases were selected were a sufficiently high number of experimental data points are available. In general, the available experimental data is more numerous for proton induced reactions and scarce in case of pions.

Figure 3 furthermore shows the calculated FLUKA cross-sections together with the experimental data and gives the ratio of the two as a function of energy. Average values can be extracted assuming a uniform contribution of the cross-section in energy and are shown in the graph as “Average Ratio”. However, for a final conclusion for any application the respective shape of the energy dependent spectra has to be taken into account when applying these ratios.

In order to judge the agreement between measured and calculated values of residual activation in case of a mixed energy spectra, those average values have to be newly calculated based on the actual particle energy spectra, thus can be significantly different than the presented results. It shall thus be noted that the current comparison focuses rather on the general method without giving a detailed analysis for all isotopes, *e.g.* those relevant for a waste characterisation at hadron accelerators (*e.g.* the LHC). For the latter detailed studies will be necessary taking into account the respective irradiation history in order to judge the influence of build-up and decay; the irradiation conditions in order to deduce the final shape of particle spectra; the detailed chemical composition of studied materials in order to define important trace elements.

Figure 3: Comparison of experimental and calculated energy-dependent production cross-sections for the selected representative isotopes of this study

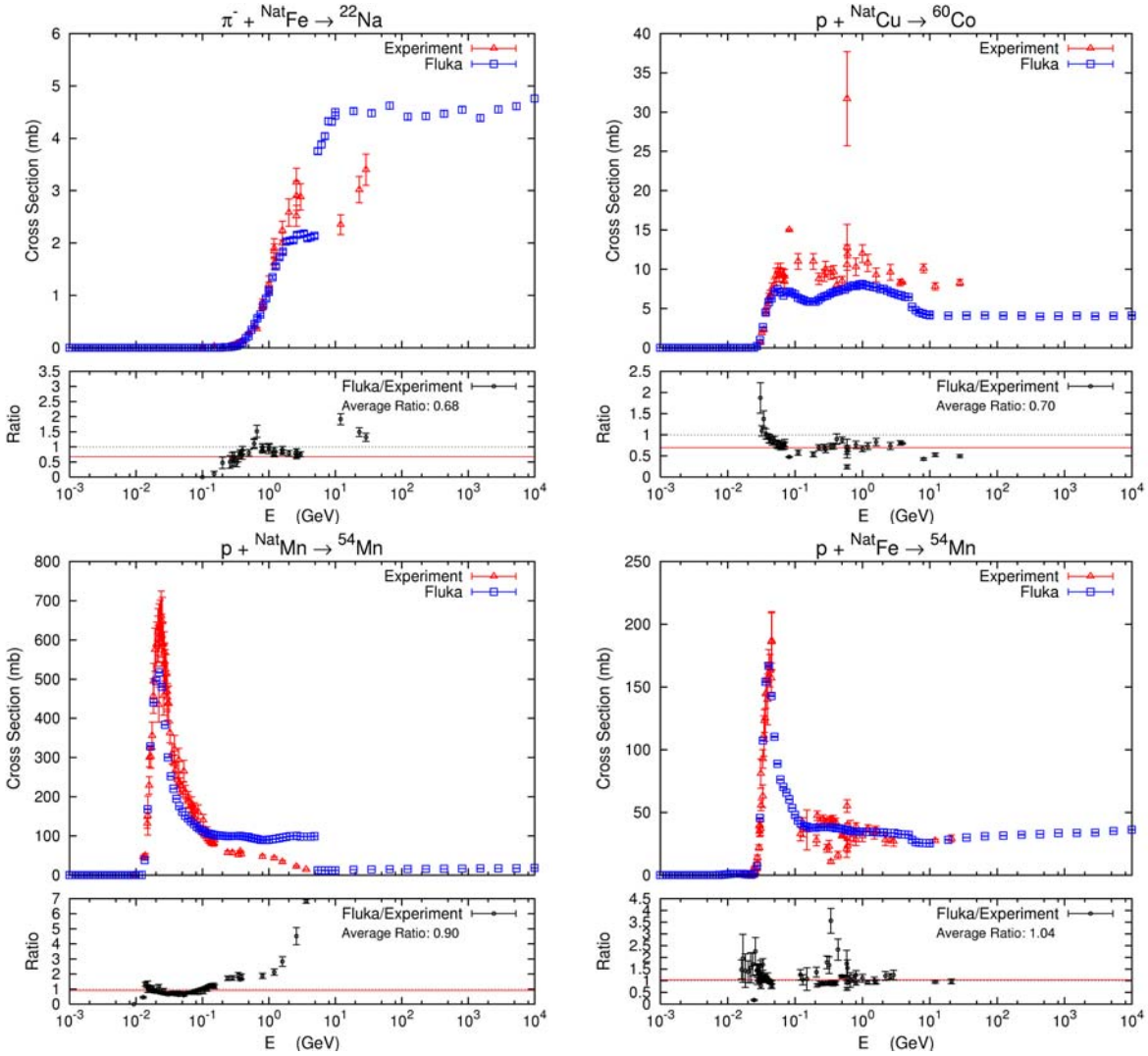

For all other channels a more automated approach is attempted in which energy-averaged ratios of measured and calculated cross-sections are computed as shown in Figure 3. As mentioned before, these ratios are not meant to allow unambiguous conclusions but should give at least an indication on the performance of FLUKA for single reaction channels.

Table 2 (for proton-induced reactions) and Table 3 (for pion-induced reactions) show a comparison for all isotopes and target materials where experimental cross-sections are available, including the respective average ratio between FLUKA cross-sections and experimental ones, together with further information on the available experimental data, thus their number and energy range. Please note that isotopes showing an error which exceeds 40% were not taken into account.

It can be seen that such a comparison can only give a first quantitative picture with the further need to make a deeper analysis for the isotopes important for the relevant study. This is supported by the fact of the observed good agreements between measurements and simulations as performed at CERF. The results presented in Tables 2 and 3 can further be used to compare the calculated FLUKA production cross-sections and the available experimental data collection with the experimental data obtained at the CERF facility at CERN [3,5,8,9]. Together with the information on production channels, the respective half-life of the isotope this results in a comparison as shown for copper as example in Table 4.

The latter table shows gives for selected target materials, all produced isotopes, their half-lives, and the respective projectile, the following information:

- the isotope ratios assumed in the natural composition of the simulation;
- the respective production reaction channels;
  - *"s"* … spallation;
  - *"H"* … tritium;
  - *"n"* … neutron;
  - *"a"* … alpha;
  - *"p"* … proton;
- *"Land"* … average ratios between FLUKA and Landolt Börnstein data [4];
- *"#ofDp"* … number of available data in the Landolt Börnstein compendium;
- *"CERF"* … ratios observed during the CERF experiments [3,5,8,9].

This preliminary study shows the clear need to further compare on a detailed basis the available experimental data, the results as obtained at CERF and the currently available data for isotope production cross-sections as calculated with FLUKA. With respect to the application for the radioactive waste this has to be done for all isotopes of interest and will finally lead to a quantification of the underlying uncertainties in both, simulations and experiment.

Typical particle spectra for the LHC

Due to the complexity and heterogeneity of the LHC machine, finding one representative radiation field which can be used for the assessment of any radiological quantity is not possible. However, for one area and its associated beam loss mechanisms, it is possible to calculate with FLUKA any particle spectra which can be used for the calculation of such quantities. In the case of the presented application to the radioactive waste, it is sufficient to limit the spectra calculation to protons, neutrons and pions for which the production cross-sections were computed as explained before.

A detailed description of the beam cleaning insertion where an important fraction of the protons from the beam are lost was thus used to investigate the sensitivity of radioactive nuclei production to specific characteristics of the radiation field such as the distance and shielding between the loss points and the object of interest. The FLUKA geometry includes the beam line components such as the collimators, dipole and quadrupole magnets as well as the tunnel structure. Figure 6 shows the distribution of collimators and magnets along the beam pipe on a longitudinal cut of the FLUKA geometry.

The spectra were scored at the different locations of the collimators or magnets leading to the calculation of 400 different spectra. The collimators are represented by two carbon jaws surrounded by a water layer and a copper cooling plate both enclosed in a steel tank. Particle spectra were scored in the jaws in which the 7 TeV beam particles interact as well as in the water. The magnets are represented using a simplified layout including the steel yoke, one copper and one water ring representing the coils and the water cooling system. The spectra were scored in the yoke as well as in the water. A cut of collimators and magnets as they are implemented in the FLUKA geometry and the locations where the spectra are scored is shown in Figure 7.

For the tunnel structure, a realistic configuration is implemented in the FLUKA geometry. Spectra were scored in the floor of the tunnel, in the walls and in the air; the latter two were divided into three different sections for scoring purposes. Furthermore, spectra were also calculated in the different water pipes which go through the beam cleaning insertions. A cut of the tunnel perpendicular to the beam axis is represented in Figure 8.

It has to be noted that the spectra calculation is performed with FLUKA using a track length estimator, thus the scored quantity corresponds to the average over an extended object and do not reflect the possible heterogeneity of the field insight the object. For example, in the case of the floor or of the water pipes, the spectra can locally be very different close to a loss point from the spectra which are averaged over the entire length of the beam cleaning insertion.

Table 2: Overall comparison (FLUKA/experiment) of proton-induced experimental [4] and with FLUKA calculated energy-dependent production cross-sections for all isotopes where experimental data were available (statistical error below 40%)

In addition to the average ratio and its error also the number of available data points as well as their energy range is shown

Target	Isotope	Average Ratio	Error [%]	Number of Data Points	minimum Energy [GeV]	maximum Energy [GeV]	Average Energy [GeV]	Target	Isotope	Average Ratio	Error [%]	Number of Data Points	minimum Energy [GeV]	maximum Energy [GeV]	Average Energy [GeV]
Al	I13	0.413	26.673	23	0.016	25.000	2.017	Fe	Sc49	0.611	15.538	6	0.500	12.000	3.150
Al	Be7	2.863	15.660	143	0.028	300.000	2.890	Fe	V48	0.933	12.893	46	0.039	21.000	1.251
Al	Be10	3.370	13.381	34	0.057	1.200	0.323	Fe	Cr48	1.545	21.541	6	0.150	12.000	2.485
Al	C11	1.301	6.304	11	0.400	300.000	31.356	Fe	Cr51	0.318	19.201	40	0.013	21.000	0.651
Al	Na22	1.127	13.055	312	0.022	300.000	1.337	Fe	Mn52	3.174	16.173	4	0.024	12.000	3.281
Al	Na24	0.346	13.996	216	0.010	300.000	2.122	Fe	Mn54	1.035	15.705	69	0.016	21.000	0.856
Ca	Na22	0.719	10.296	13	0.168	24.000	2.836	Fe	Mn56	0.585	39.707	5	0.150	12.000	2.862
Ca	Na24	0.371	15.606	11	0.100	2.600	1.073	Fe	Fe52	0.972	18.787	11	0.019	12.000	1.076
Ca	Mg28	0.337	27.614	5	1.200	2.600	1.840	Fe	Fe53	0.331	36.762	2	0.150	0.660	0.405
Ca	Cl36	0.887	13.641	8	0.150	24.000	3.591	Fe	Co55	1.098	15.262	66	0.013	12.000	0.311
Ca	K42	0.974	18.017	5	1.200	2.600	1.840	Fe	Co56	0.613	14.532	255	0.005	21.000	0.235
Ca	K43	1.606	12.864	7	0.800	2.600	1.543	Mg	Be7	1.188	15.800	52	0.042	23.000	1.047
C	H3	1.268	14.422	14	0.150	6.200	1.533	Mg	Be10	1.606	14.365	22	0.062	23.000	1.901
C	Be7	0.949	11.240	174	0.025	300.000	2.820	Mg	Na22	1.094	10.906	119	0.006	24.000	0.940
C	Be10	0.997	12.400	17	0.031	1.600	0.207	Mg	Na24	0.603	13.499	98	0.018	2.900	0.244
C	C11	0.631	4.507	189	0.018	300.000	2.517	Mn	Be7	1.164	16.215	11	0.282	2.600	1.129
Co	Be7	1.293	16.240	17	0.277	12.000	2.316	Mn	Be10	1.432	26.475	15	0.059	2.600	0.714
Co	Be10	1.121	22.354	4	0.233	0.380	0.308	Mn	Na22	0.670	22.350	19	0.100	2.600	1.050
Co	Na22	0.410	35.056	25	0.100	12.000	1.349	Mn	Na24	0.442	36.966	6	0.100	3.650	1.592
Co	Na24	0.466	20.727	13	0.100	12.000	2.616	Mn	Mg28	0.490	24.040	4	1.200	3.650	2.263
Co	Mg28	0.339	21.313	6	1.000	12.000	5.325	Mn	Cl36	0.664	9.774	4	0.239	0.384	0.313
Co	P32	0.911	22.024	4	1.760	2.750	2.253	Mn	K43	0.401	14.251	9	0.239	3.650	1.234
Co	Cl36	0.789	16.583	4	0.233	0.380	0.308	Mn	Sc46	0.513	9.303	10	0.239	3.650	1.170
Co	K42	0.665	16.126	12	0.150	18.300	4.128	Mn	Sc47	0.858	17.182	21	0.076	3.650	0.314
Co	K43	0.540	17.362	17	0.150	18.300	3.456	Mn	Sc48	0.921	30.355	21	0.076	3.650	0.314
Co	Sc44	1.818	9.951	4	0.500	12.000	4.288	Mn	V48	0.824	11.505	37	0.047	3.650	0.407
Co	Sc46	0.499	10.642	24	0.170	12.000	1.712	Mn	Cr48	2.162	34.667	25	0.061	3.650	0.292
Co	Sc48	1.017	16.054	9	0.500	12.000	3.739	Mn	Cr51	0.697	9.995	62	0.016	3.650	0.252
Co	Cr48	1.428	20.827	21	0.069	12.000	1.752	Mn	Mn52	1.806	12.256	45	0.027	3.650	0.328
Co	Cr51	0.666	9.735	58	0.049	12.000	0.762	Mn	Mn54	0.899	9.977	75	0.009	3.650	0.195
Co	Mn52	1.214	13.155	51	0.049	12.000	0.435	Mn	Fe52	1.457	16.118	83	0.038	3.650	0.130
Co	Fe52	1.167	19.973	32	0.062	3.650	0.234	Na	Be7	2.668	17.412	17	0.031	5.700	0.434
Co	Co55	1.149	17.288	50	0.042	12.000	0.735	Na	Na22	1.187	10.595	38	0.015	5.700	0.252
Co	Co56	1.275	11.928	98	0.027	12.000	0.468	Ni	Be7	1.459	17.022	29	0.065	23.000	2.274
Co	Co57	0.366	10.997	136	0.012	12.000	0.329	Ni	Be10	1.200	34.260	23	0.053	2.600	0.545
Co	Co58	1.329	8.359	64	0.012	12.000	0.646	Ni	Na22	0.611	25.276	21	0.100	23.000	2.610
Co	Ni56	1.919	26.240	25	0.038	1.600	0.140	Ni	Na24	0.410	26.475	17	0.100	12.000	2.800
Co	Ni57	2.706	12.529	93	0.019	12.000	0.283	Ni	Mg28	0.297	29.588	3	3.650	12.000	8.217
Cr	Cr51	4.348	6.919	17	0.014	0.600	0.051	Ni	P32	0.970	33.458	9	0.130	2.900	1.009
Cr	Mn52	4.634	15.615	17	0.006	0.600	0.032	Ni	Cl36	0.611	13.640	6	0.230	1.200	0.537
Cu	H3	1.305	33.185	4	0.660	25.000	15.665	Ni	K42	0.411	14.642	7	0.500	12.000	4.364
Cu	Be7	1.331	14.867	30	0.065	30.000	4.868	Ni	K43	0.368	17.651	7	0.500	12.000	4.364
Cu	Na22	0.463	23.821	22	0.100	30.000	8.092	Ni	Sc43	1.040	13.095	4	0.500	2.000	3.788
Cu	Na24	0.476	21.312	45	0.050	800.000	40.155	Ni	Sc44	1.894	11.896	4	0.500	12.000	6.288
Cu	Mg28	0.546	20.605	7	1.000	400.000	63.550	Ni	Sc46	0.491	11.113	19	0.211	12.000	1.923
Cu	P32	2.562	30.069	5	0.120	24.000	4.303	Ni	Sc47	0.322	20.317	9	0.500	12.000	3.550
Cu	Ar39	0.422	12.328	12	0.540	29.000	14.141	Ni	Sc48	0.348	27.585	3	9.000	12.000	8.217
Cu	Ar42	0.737	26.288	9	0.600	29.000	13.239	Ni	V48	1.644	23.605	9	0.130	2.900	0.992
Cu	K42	0.637	15.167	23	0.150	400.000	26.735	Ni	Cr48	2.744	23.633	4	0.500	12.000	6.288
Cu	K43	0.583	19.582	26	0.150	30.000	8.496	Ni	Cr51	0.673	15.764	17	0.036	9.000	1.656
Cu	Ca47	1.030	38.768	3	1.600	24.000	12.533	Ni	Mn52	0.435	13.431	36	0.036	12.000	1.473
Cu	Sc43	0.656	21.272	5	0.500	24.000	8.230	Ni	Mn54	0.748	12.045	33	0.041	12.000	1.334
Cu	Sc44	1.513	9.139	9	0.500	28.000	9.082	Ni	Mn56	0.228	23.558	4	0.500	12.000	6.288
Cu	Sc46	0.555	9.526	26	0.200	28.000	3.699	Ni	Fe52	0.706	14.600	49	0.045	12.000	0.608
Cu	Sc48	0.160	17.965	26	0.200	28.000	3.646	Ni	Fe59	0.591	25.872	13	0.211	12.000	1.601
Cu	V48	0.640	10.553	27	0.090	400.000	18.331	Ni	Co55	0.504	13.044	132	0.005	12.000	0.311
Cu	Cr49	1.133	20.510	7	0.184	24.000	3.729	Ni	Co56	1.246	14.083	71	0.016	9.000	0.373
Cu	Cr51	0.557	9.077	26	0.110	28.000	3.634	Ni	Co57	3.104	11.858	138	0.005	12.000	0.311
Cu	Mn52	1.112	9.755	35	0.065	400.000	14.154	Ni	Co58	0.988	12.219	15	0.024	12.000	1.423
Cu	Mn54	0.812	8.885	39	0.046	28.000	2.486	Ni	Co60	1.088	15.937	13	0.211	2.600	0.724
Cu	Mn56	0.632	12.778	14	0.090	28.000	5.913	Ni	Ni56	0.542	19.239	49	0.018	12.000	0.847
Cu	Fe52	1.130	25.478	22	0.090	30.000	6.377	O	Be7	0.610	15.303	119	0.030	19.000	0.709
Cu	Fe59	0.546	16.856	45	0.049	30.000	3.307	Si	H3	0.056	21.429	7	0.021	3.000	0.538
Cu	Co55	1.171	13.843	52	0.070	30.000	2.817	Si	Be7	1.383	17.456	109	0.031	24.000	0.766
Cu	Co56	1.150	12.226	84	0.044	30.000	1.794	Si	Be10	2.336	22.255	33	0.050	23.000	1.258
Cu	Co57	0.883	11.540	93	0.026	30.000	1.591	Si	Na22	0.895	16.465	165	0.018	24.000	0.693
Cu	Co58	0.814	10.267	92	0.026	30.000	1.632	Si	Na24	0.453	16.664	89	0.026	2.900	0.308
Cu	Co60	0.699	11.159	41	0.031	28.000	1.679	Si	Al28	0.520	20.469	20	0.018	0.103	0.056
Cu	Co61	0.900	16.107	11	0.090	30.000	10.211	Ti	Sc44	1.037	13.870	24	0.013	12.000	0.547
Cu	Ni56	0.808	34.693	54	0.058	28.000	1.046	Ti	Sc47	1.005	15.081	33	0.011	0.584	0.067
Cu	Ni57	1.901	11.498	102	0.041	28.000	1.389	Zn	Be7	1.380	20.555	2	0.500	12.000	6.250
Cu	Cu60	0.944	15.453	57	0.036	30.000	1.611	Zn	K42	0.663	20.393	2	0.500	12.000	6.250
Cu	Cu61	0.779	17.061	51	0.020	30.000	2.522	Zn	K43	1.045	22.364	2	0.500	12.000	6.250
Cu	Cu64	0.950	11.154	38	0.016	28.000	1.018	Zn	Sc44	2.699	14.773	2	0.500	12.000	6.250
Cu	Zn61	0.473	29.751	6	0.030	0.047	0.038	Zn	Sc46	0.815	15.314	2	0.500	12.000	6.250
Cu	Zn62	0.938	13.524	73	0.011	28.000	1.004	Zn	Sc47	0.809	36.730	2	0.500	12.000	6.250
Cu	Zn63	0.782	15.003	83	0.005	28.000	0.419	Zn	V48	1.092	13.164	2	0.500	12.000	6.250
Fe	H3	1.686	31.897	4	0.130	25.000	12.645	Zn	Cr48	2.063	24.336	2	0.500	12.000	6.250
Fe	Be7	1.408	17.892	39	0.085	24.000	2.882	Zn	Cr51	0.668	12.628	2	0.500	12.000	6.250
Fe	Be10	1.329	26.897	26	0.058	2.600	0.674	Zn	Mn52	1.593	12.963	2	0.500	12.000	6.250
Fe	Na22	0.663	19.782	34	0.100	29.000	2.691	Zn	Mn54	0.775	12.392	2	0.500	12.000	6.250
Fe	Na24	0.305	23.716	22	0.100	29.000	4.017	Zn	Mn56	0.843	19.601	2	0.500	12.000	6.250
Fe	Mg28	0.479	25.735	6	0.150	12.000	2.744	Zn	Fe59	0.536	19.952	2	0.500	12.000	6.250
Fe	P32	0.822	26.442	12	0.130	2.900	0.858	Zn	Co55	1.662	19.840	2	0.500	12.000	6.250
Fe	Cl36	0.691	17.283	10	0.150	24.000	3.045	Zn	Co56	1.455	12.726	2	0.500	12.000	6.250
Fe	Ar39	0.339	15.449	5	0.430	25.000	10.280	Zn	Co57	0.930	31.804	2	0.500	12.000	6.250
Fe	K42	0.533	15.965	15	0.150	29.000	6.257	Zn	Co58	0.835	12.447	2	0.500	12.000	6.250
Fe	K43	0.560	20.613	20	0.150	29.000	3.612	Zn	Co60	0.697	15.661	2	0.500	12.000	6.250
Fe	Ca45	0.756	37.113	2	0.150	0.660	0.405	Zn	Ni57	2.122	16.232	2	0.500	12.000	6.250
Fe	Sc43	0.765	22.043	5	0.150	12.000	2.862	Zn	Cu61	1.258	17.585	2	0.500	12.000	6.250
Fe	Sc44	1.129	16.489	5	0.150	12.000	2.862	Zn	Zn62	0.995	13.974	2	0.500	12.000	6.250
Fe	Sc46	0.543	11.105	21	0.150	12.000	1.182	Zn	Zn65	0.507	12.845	2	0.500	12.000	6.250
Fe	Sc47	1.259	25.809	12	0.120	2.900	0.899								

Table 3: Overall comparison of pion-induced experimental [4] and with FLUKA calculated energy-dependent production cross-sections for all isotopes where experimental data were available (statistical error below 40%)

In addition to the average ratio and its error also the number of available data points as well as their energy range is shown

Projectile: Posive Pions								Projectile: Negative pions							
Target	Isotope	Average Ratio	Error [%]	Number of Data Points	minimum Energy [GeV]	maximum Energy [GeV]	Average Energy [GeV]	Target	Isotope	Average Ratio	Error [%]	Number of Data Points	minimum Energy [GeV]	maximum Energy [GeV]	Average Energy [GeV]
AlNat	*Na24*	0.438	6.752	18	0.050	0.389	0.186	*AlNat*	*C11*	1.002	18.487	6	0.450	1.760	1.107
CNat	*C11*	0.915	7.099	68	0.030	0.550	0.196	*AlNat*	*Na22*	0.929	16.577	7	0.069	0.285	0.176
CuNat	*V48*	0.683	18.187	4	0.050	0.350	0.173	*AlNat*	*Na24*	0.450	6.267	24	0.050	0.500	0.204
CuNat	*Cr49*	0.891	39.969	4	0.050	0.350	0.173	*CNat*	*C11*	1.432	7.145	130	0.030	2.360	0.657
CuNat	*Cr51*	0.502	23.002	4	0.050	0.350	0.173	*CuNat*	*Sc46*	0.557	35.848	3	0.100	0.350	0.213
CuNat	*Mn52*	1.026	16.424	5	0.050	0.350	0.151	*CuNat*	*V48*	0.824	24.889	4	0.050	0.350	0.173
CuNat	*Mn54*	0.622	17.898	4	0.050	0.350	0.173	*CuNat*	*Cr49*	1.000	34.267	4	0.050	0.350	0.173
CuNat	*Mn56*	0.536	18.510	5	0.050	0.350	0.151	*CuNat*	*Cr51*	0.615	19.335	4	0.050	0.350	0.173
CuNat	*Fe52*	0.791	30.550	5	0.050	0.350	0.151	*CuNat*	*Mn52*	1.100	21.592	5	0.050	0.350	0.151
CuNat	*Co55*	0.982	19.878	4	0.050	0.350	0.173	*CuNat*	*Mn54*	0.590	16.412	4	0.050	0.350	0.173
CuNat	*Co56*	0.880	26.479	4	0.050	0.350	0.173	*CuNat*	*Mn56*	0.547	19.484	5	0.050	0.350	0.151
CuNat	*Co57*	0.771	15.086	4	0.050	0.350	0.173	*CuNat*	*Fe59*	0.670	28.886	5	0.050	0.350	0.151
CuNat	*Co58*	0.760	13.365	4	0.050	0.350	0.173	*CuNat*	*Co55*	1.023	21.373	4	0.050	0.350	0.173
CuNat	*Co61*	0.991	29.983	4	0.050	0.350	0.173	*CuNat*	*Co56*	0.837	27.433	4	0.050	0.350	0.173
CuNat	*Ni57*	1.480	20.580	5	0.050	0.350	0.151	*CuNat*	*Co57*	0.839	17.850	4	0.050	0.350	0.173
CuNat	*Cu61*	1.113	13.646	4	0.050	0.350	0.173	*CuNat*	*Co58*	0.809	14.338	4	0.050	0.350	0.173
CuNat	*Zn62*	1.431	25.742	5	0.050	0.350	0.151	*CuNat*	*Co61*	0.926	22.295	4	0.050	0.350	0.173
								CuNat	*Ni57*	1.713	28.735	5	0.050	0.350	0.151
								CuNat	*Cu61*	1.089	16.858	4	0.050	0.350	0.173
								FeNat	*Sc46*	0.621	13.081	5	0.060	0.278	0.140
								FeNat	*Mn54*	0.677	11.549	5	0.060	0.278	0.140
								SiNat	*Na24*	0.354	7.148	22	0.050	0.500	0.220

Table 4: Comparison of all available cross-section data for natural copper as target material

The table shows (columns from left to right) the produced isotope, its half life, the respective projectile (p…proton, pi+…positively charged pion, pi-…negatively charged pion), the isotope ratios of the natural composition (including the respective ratio in per cent) and its reaction channels (s…spallation, t…tritium, n…neutron, a…alpha, p…proton) as well as ratios observed as average values for the data compendium [4] and the experiments performed at CERF [3,5,8,9].

Isotope	Half Life	Proj	29Cu63 69	Cu65 31	Land.	# of D P.	CERF	Isotope	Half Life	Proj	29Cu63 69	Cu65 31	Land.	# of D P.	CERF	Isotope	Half Life	Proj	29Cu63 69	Cu65 31	Land.	# of D P.	CERF
Be7	**53.29d**	p	s	s	1.33	30				p	s	s	0.64	27	1.16			p	s	s	1.15	84	1.04
Na22	**2.603a**	p	s	s	0.46	22	0.72	**V48**	**15.97d**	pi+	s	s	0.68	4		**Co56**	**77.26d**	pi+	s	s	0.88	4	
Na24	**14.96h**	p	s	s	0.47	45	0.42			pi-	s	s	0.83	4				pi-	s	s	0.84	4	
Mg28	**20.9h**	p	s	s	0.55	7	0.25	**Cr48**	**21.6h**	pi+	s	s	0.86	4	0.92			p	s	s	0.88	93	0.85
Al28	**2.246m**	n	s	s	0.25					p	s	s	1.13	7	1	**Co57**	**271.79d**	pi+	s	s	0.77	4	
P32	**14.26d**	p	s	s	2.56	5		**Cr49**	**42m**	pi+	s	s	0.89	4				pi-	s	s	0.84	4	
S38	**2.83h**	p	s	s	1.02	2				pi-	s	s	1	4				p	s	s	0.81	92	0.91
Cl39	**56m**	p	s	s	0.47	2				p	s	s	0.56	26	1.06	**Co58**	**70.86d**	pi+	s	s	0.76	4	
Cl39	**56m**	p	s	s	0.42	12		**Cr51**	**27.7d**	pi+	s	s	0.5	4				pi-	a	s	0.81	4	
Ar41	**1.83h**	p	s	s	0.45	2	0.39			pi-	s	s	0.62	4		**Co60**	**5.272a**	p	pap	s	0.7	41	0.9
		pi+	s	s	0.27	2				p	s	s	1.11	35	0.68			p	s	pap	0.9	11	0.68
Ar42	**33a**	p	s	s	0.74	9		**Mn52**	**5.6d**	pi+	s	s	1.03	5		**Co61**	**1.65h**	pi+	s	a	0.99	4	
K42	**12.36h**	p	s	s	0.64	23	0.66			pi-	s	s	1.1	5				pi-	a	a	0.93	4	
		pi-	s	s	0.49	2				p	s	s	0.81	39	1.13	**Ni56**	**6.075d**	p	s	s	0.81	54	
K43	**22.2h**	p	s	s	0.58	26	0.81	**Mn54**	**312.2d**	pi+	s	s	0.62	4				p	s	s	1.9	102	0.76
		pi+	s	s	0.63	2				pi-	s	s	0.59	4		**Ni57**	**36.0h**	pi+	s	s	1.48	5	
		pi-	s	s	0.65	3				p	s	s	0.64	14	0.81			pi-	s	s	1.71	5	
Ca47	**4.54d**	p	s	s	1.03	3	0.59	**Mn56**	**2.58h**	pi+	s	s	0.54	5		**Ni65**	**2.52h**	n	/	np	1.46		
Sc43	**3.89h**	p	s	s	0.66	5	0.4			pi-	s	s	0.55	5		**Cu60**	**23m**	p	ptn	s	0.94	57	0.78
Sc44	**3.92h**	p	s	s	1.51	9	0.89	**Fe52**	**8.27h**	p	s	s	1.13	22				p	pt	s	0.78	51	0.87
Sc46	**83.82d**	p	s	s	0.55	26	0.81			pi+	s	s	0.79	5		**Cu61**	**3.4h**	pi+	a	s	1.11	4	
		pi+	s	s	0.67	3		**Fe59**	**44.5d**	p	s	s	0.55	45	0.82			pi-	-2n	s	1.09	4	
		pi-	s	s	0.56	3				pi+	s	s	0.51	4		**Cu64**	**12.7h**	p	/	pd	0.95	38	0.63
Sc47	**3.35d**	pi+	s	s	0.58	4	1.09			pi-	a	s	0.67	5		**Zn62**	**9.13h**	p	p2n	s	0.94	73	1.05
Sc48	**43.67h**	p	s	s	0.16	26	1.39	**Co55**	**17.54h**	p	s	s	1.17	52	0.66			pi+	+2n	s	1.43	5	
		pi+	s	s	0.67	3				pi+	s	s	0.98	4		**Zn65**	**244.3d**	n	/	/	0.97		
		pi-	s	s	0.69	4				pi-	s	s	1.02	4									

Figure 6: Cross-section of the FLUKA geometry used to simulate the hadronic cascade development induced by proton losses in the collimators

Stars indicate the locations where particle spectra were scored

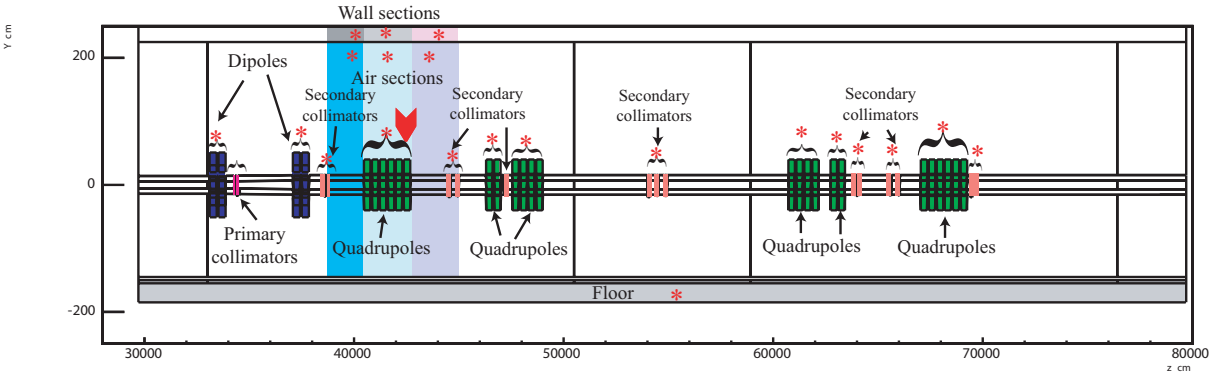

Figure 7: Cross-sectional view of a quadrupole (left) and a collimator (right)

The locations where the spectra are scored are indicated with red stars

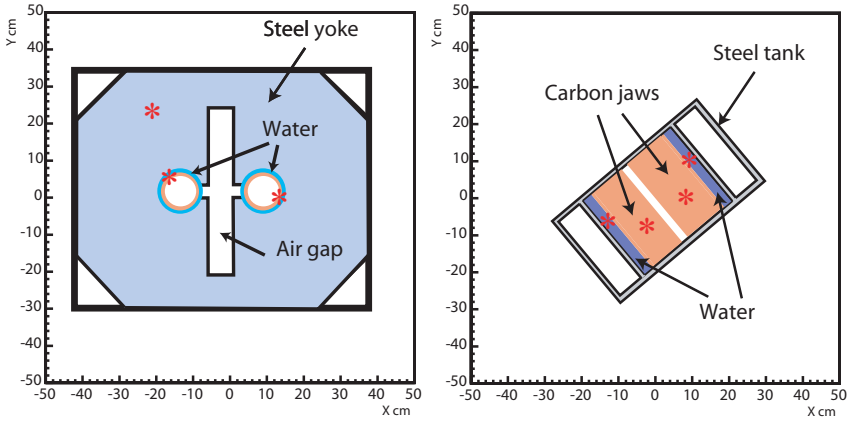

Figure 8: Cross-section of the tunnel geometry perpendicular to the beam axis

The locations where spectra are scored are indicated with stars

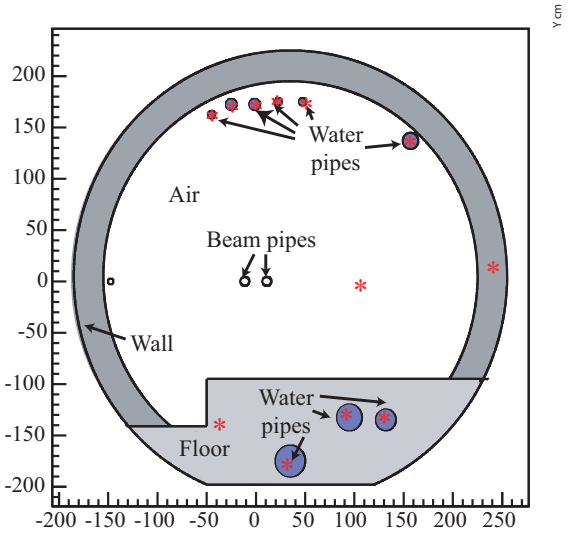

Several criteria can be defined to compare a set of spectra (in our case for four particle types) to another one at a different location. The strategy which is chosen here is to limit the study to changes in shape without taking into account the intensity which strongly depends on the distance between the region of interest and the loss points (collimators). Consequently, in a first step the spectra set is normalised to unity. The four energy spectra are integrated and the sum allows the determination of the normalisation factor.

It has to be noted that the neutron spectrum is treated in a specific way since in FLUKA the transport of neutrons below 19.6 MeV is performed using a multi-group transport algorithm and (if available) evaluated isotope production cross-sections. In this study, for the calculation of radioactive nuclei production, these low-energy neutron cross-sections were extracted from the code and folded separately with the neutron respective spectra below 19.6 MeV.

Once the sum of the fluences of protons, neutrons (above 19.6 MeV), positive pions and negative pions is normalised to unity, instead of comparing the shapes of different spectra sets for all energies, they are first multiplied with production cross-sections to limit the comparison to the part of the spectra where cross-sections are significant.

Table 5: Radioactive nuclei production calculated for the five different reactions (ranging from "low" to "high" energies reaction channels) and different locations selected out of the numerous studied spectra sets considered

The production calculated in the CERF samples is also indicated, the one in the lateral sample was used for the final normalisation of the results. Please note that for the water cooling the case for the first primary collimator is special in the sense that the cascade does not yet reach a maximum in the collimator, thus leads to particle spectra shifted to lower energies.

	Mn54_Mn	Mn54_Fe	Co60_Cu	Na22__Fe	Be7_Cu
Wall 1St Section	1.08E+00	1.14E+00	1.09E+00	4.78E-01	4.41E-01
Wall 3rd Section	1.15E+00	1.16E+00	1.09E+00	4.93E-01	4.41E-01
Pipe in the Floor	1.23E+00	1.34E+00	1.27E+00	1.13E-01	1.12E-01
1St Quad. Yoke	1.15E+00	1.19E+00	1.09E+00	4.93E-01	4.41E-01
Last Quad. Yoke	1.23E+00	1.25E+00	1.18E+00	3.48E-01	3.24E-01
Pipe in the air	1.00E+00	1.03E+00	1.00E+00	7.25E-01	6.76E-01
1St Quad. Water	1.00E+00	1.03E+00	1.00E+00	8.55E-01	7.65E-01
Last Quad. Water	1.00E+00	9.69E-01	1.00E+00	9.57E-01	8.82E-01
2nd Air section	9.23E-01	9.06E-01	9.00E-01	1.41E+00	1.26E+00
Beam pipe 2nd section	9.23E-01	8.59E-01	8.82E-01	1.33E+00	1.21E+00
1St Prim. Coll. Water	9.23E-01	9.38E-01	1.00E+00	6.38E-01	5.29E-01
2nd Prim. Coll. Water	7.46E-01	7.50E-01	8.09E-01	1.74E+00	1.41E+00
3rd Prim. Coll. Water	7.46E-01	7.50E-01	8.00E-01	1.74E+00	1.44E+00
2nd Second. Coll. Water	7.46E-01	7.34E-01	7.91E-01	1.74E+00	1.56E+00
3rd Second. Coll. Water	7.46E-01	7.19E-01	7.82E-01	1.74E+00	1.59E+00
Last Second. Coll. Water	7.69E-01	7.50E-01	8.18E-01	1.59E+00	1.44E+00
Beam pipe 1st section	5.31E-01	5.63E-01	6.18E-01	2.75E+00	2.41E+00
2nd Primary jaws	4.92E-01	5.47E-01	6.09E-01	2.90E+00	2.38E+00
1St Secondary jaws	6.00E-01	6.09E-01	6.82E-01	2.46E+00	2.15E+00
Last Secondary jaws	5.85E-01	5.94E-01	6.64E-01	2.46E+00	2.21E+00
CERF Downstream	5.69E-01	6.09E-01	6.64E-01	2.75E+00	2.44E+00
CERF Lateral	1.00E+00	1.00E+00	1.00E+00	1.00E+00	1.00E+00

Five different reactions are considered to take into account different reaction channels. Cross-sections were selected based on the physics mechanism involved or on the contribution of the produced isotope to the activity in the waste after significant cooling times. Those cross-sections are, ranging from the ones which can be qualified as being important at low energies to the ones dominating at higher energies, Mn54 produced respectively on Mn and Fe, Co60 produced on Cu, Na22 produced on Fe and Be7 produced on Cu.

For each reaction, the four response spectra are then integrated and the sum corresponds to the number of radioactive nuclei produced per cm of hadron track length and by units of volume. In order to validate, the general method presented here for waste calculations and particularly the relevance of the experimental verification of the FLUKA predictions, the spectra were also compared to the representative spectra in the samples which were irradiated in the CERF facility. The same procedure

described for the spectra calculated in the beam cleaning insertion is applied to two spectra sets corresponding to samples located respectively laterally and downstream the target. A part of the results obtained for the numerous studied locations is presented in Table 5 for the four reactions which were considered. The production is normalised to the one calculated in the CERF sample located laterally from the target in order to facilitate the comparison between the different locations and the CERF results.

Since the calculation of radioactive nuclei production for waste characterisation does not require a very high accuracy the spectra sets calculated in the beam cleaning insertion can be subdivided into four main groups by using the values as calculated for the five reactions (see Table 5). For each group one representative spectra set is selected and can then be used for the calculation of radioactive nuclei production at any location.

The four representative spectra sets can be characterised by the relative contribution of neutrons, protons and pions to the radionuclide production. The relative contribution is also strongly correlated to possible energy peaks of the respective spectra, *e.g.* of the positive and negative pions in the intermediate energy range or the neutron and proton spectra showing a maximum around 100 MeV and 200 MeV respectively in all cases.

a) The first representative spectra set is the one scored in the yoke of the first quadrupole magnet module situated after the first secondary collimators. The hadronic radiation field is dominated by neutrons. Charged hadrons account only for approximately 20% of the isotope production. In terms of radioactive nuclei production, this spectrum is found representative of the situation inside the walls and floor or of pipes buried in the floor.

b) The second representative spectra set is the one scored in the water ring surrounding the copper beam pipe. The hadronic field is rather similar than in the previous case except that the charged hadrons contribution is relatively more important and peaked at a higher energy.

c) The third representative spectra set is scored in the water layer representing the cooling system of the first secondary collimator jaw. The contribution of the four hadron types considered is more or less equivalent in this case.

d) The last spectrum set represents the extreme case of an object which would be located very close to the beam. In this case, positive and negative pion contributions are dominant and peaked at an even higher energy than in the previous case. This spectrum is representative of radioactive nuclei production very close or inside to the beam and consequently to the loss points.

The two first representative spectra appear to be similar in their shape to the CERF spectra located laterally to the beam target while the two other spectra sets correspond to an intermediate situation between the spectra calculated laterally and downstream of the CERF target. The locations corresponding to the same groups appear with the same colour in Table 5. The particle spectra for the different groups are represented in Figure 9.

In order to evaluate the accuracy of the method, the error which is made on the radioactive nuclei production when the representative spectra is used instead of the real one is presented in Table 6 for several extreme cases.

As an additional cross check, the same approach was studied for the part of the neutron spectra below 19.6 MeV. Several reactions like ^{108}Ag production on natural Ag, ^{57}Co on Ni, ^{60}Co production on ^{59}Co, Cu and Ni were considered. It appears that in the case of the low energy part of the neutron spectrum, finding representative spectra is less obvious than for the high energy components of the hadron field. This is due to the fact that the production of radioactive nuclei is very sensitive to possible resonances in the cross-sections. However, the same representative locations used for high energy reactions were used as a first approximation. For more accurate results a further study of additional production cross-sections should be performed. Figure 10 shows the four neutron spectra after normalisation at the four representative locations.

Table 6 shows that the disagreement reaches its maximum for reactions occurring at high energies and especially in the case of particle spectra of the first group (being sensible for source spectra at lower energies). However, in this case, radioactive nuclei induced by high energy particles will not dominate the radioactive waste considerations, thus is a good confirmation of the accuracy of the method for the selected application.

Figure 9: Particle spectra at the different representative locations, expressed in units of lethargy and after normalisation to 1 cm of hadron track length

(a) magnet yoke, (b) magnet water, (c) collimator water, (d) collimator jaw

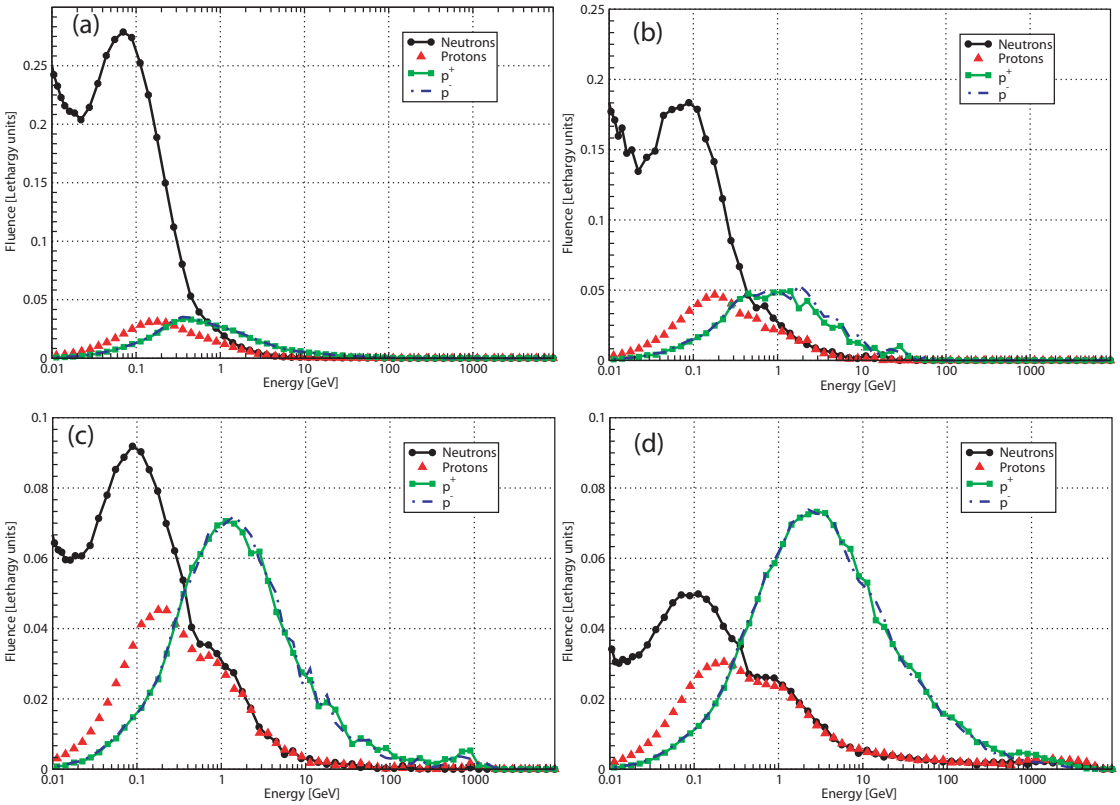

Figure 10: Neutrons spectra below 19.6 MeV at the four representative locations

Please note that due to the normalisation to the total track length spectra shown in Figure 9 cannot be directly joined

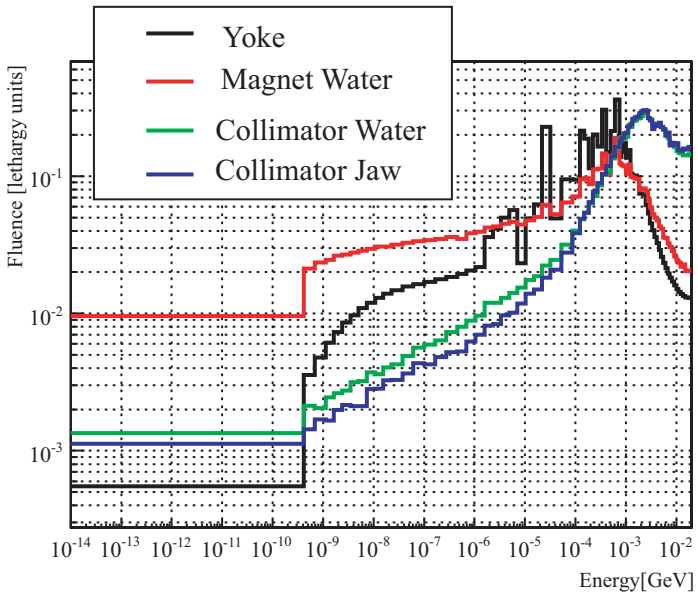

Table 6: Relative difference in per cent when comparing the isotope production as either calculated with the representative spectra or instead with the respective actual spectrum

	Mn54_Mn	Mn54_Fe	Co60_Cu	Na22__Fe	Be7_Cu
Wall 1St Section	1.08E+00	1.14E+00	1.09E+00	4.78E-01	4.41E-01
Wall 3rd Section	1.15E+00	1.16E+00	1.09E+00	4.93E-01	4.41E-01
Pipe in the Floor	1.23E+00	1.34E+00	1.27E+00	1.13E-01	1.12E-01
1St Quad. Yoke	1.15E+00	1.19E+00	1.09E+00	4.93E-01	4.41E-01
Last Quad. Yoke	1.23E+00	1.25E+00	1.18E+00	3.48E-01	3.24E-01
Pipe in the air	1.00E+00	1.03E+00	1.00E+00	7.25E-01	6.76E-01
1St Quad. Water	1.00E+00	1.03E+00	1.00E+00	8.55E-01	7.65E-01
Last Quad. Water	1.00E+00	9.69E-01	1.00E+00	9.57E-01	8.82E-01
Third Quad. Water	1.00E+00	9.69E-01	1.00E+00	9.28E-01	8.53E-01
2nd Air section	9.23E-01	9.06E-01	9.00E-01	1.41E+00	1.26E+00
Beam pipe 2nd section	9.23E-01	8.59E-01	8.82E-01	1.33E+00	1.21E+00
1St Prim. Coll. Water	9.23E-01	9.38E-01	1.00E+00	6.38E-01	5.29E-01
2nd Prim. Coll. Water	7.46E-01	7.50E-01	8.09E-01	1.74E+00	1.41E+00
3rd Prim. Coll. Water	7.46E-01	7.50E-01	8.00E-01	1.74E+00	1.44E+00
2nd Second. Coll. Water	7.46E-01	7.34E-01	7.91E-01	1.74E+00	1.56E+00
3rd Second. Coll. Water	7.46E-01	7.19E-01	7.82E-01	1.74E+00	1.59E+00
Last Second. Coll. Water	7.69E-01	7.50E-01	8.18E-01	1.59E+00	1.44E+00
1st Second. Water	7.69E-01	7.50E-01	8.09E-01	1.59E+00	1.44E+00
Beam pipe 1st section	5.31E-01	5.63E-01	6.18E-01	2.75E+00	2.41E+00
2nd Primary jaws	4.92E-01	5.47E-01	6.09E-01	2.90E+00	2.38E+00
1St Secondary jaws	6.00E-01	6.09E-01	6.82E-01	2.46E+00	2.15E+00
Last Secondary jaws	5.85E-01	5.94E-01	6.64E-01	2.46E+00	2.21E+00
CERF Downstream	5.69E-01	6.09E-01	6.64E-01	2.75E+00	2.44E+00
CERF Lateral	1.00E+00	1.00E+00	1.00E+00	1.00E+00	1.00E+00

Application to the characterisation of radioactive waste

A collection of selected cross-sections and the knowledge of how well they are reproduced by FLUKA should form the basis for the establishment of a library for the determination of the nuclide inventory of radioactive waste at CERN. The motivation for the creation of a nuclide inventory is the search for a practicable method for the classification and characterisation of radioactive waste stemmed from the CERN accelerators. Accelerator operation results in material with specific activation too high to allow it to be recycled or to be unconditionally disposed. Irrespective of the method to be used for its disposal, a detailed knowledge of the nuclide inventory in the material is essential. High accuracy is not necessarily required, but the knowledge of the tolerance in many aspects (*e.g.* chemical composition, isotope production cross-sections, etc.) is of utmost importance.

Detection of radioactivity is relatively easy but the identification and quantification of the actual nuclides in the inventory is, at best, experimentally challenging and time consuming. The selection and analysis of samples is the regular technique for linking an inventory to a waste item. However, this technique is impracticable; it is time consuming and involves too much handling of the activated material contradicting the ALARA principle. Also, as measurement techniques are specific to the class of nuclides being assayed, theoretical inventory predictions are necessary for the design of the analysis programme.

In order to characterise the radioactive waste which has been produced at CERN in the last decades, gamma-spectroscopy measurements must be accompanied by predictions of induced radioactivity. This last step is particularly important for estimating the activity of nuclides which are difficult to detect, *e.g.* ^{36}Cl and ^{55}Fe. The nuclide inventory, which depends on the material composition and irradiation history, can then be normalised to the surface dose-rate which is measured on the actual waste before packaging and/or specific isotopes being characteristic for the respective material ("fingerprints"). In this way one can complete the predictions based on our information about the waste (chemical composition and location in the accelerator) with a measurement which reflects the actual number of particles responsible for the activation. This method is usually referred to as "fingerprint method".

Decoupling the estimate of isotope production cross-sections and particle spectra is an essential simplification by allowing each to be made with calculation methods specific to their individual needs. Folding the cross-sections with the appropriate spectra results in production rates serving as basis for the calculation of total isotope produced in the respective radioactive waste.

As it regards the FLUKA predictions, the exactness of the nuclide inventory relies on the cross-sections which are predicted or used by the code, on its capability of simulating the hadronic shower and on the calculation of build-up and decay of the produced nuclides. The validation of FLUKA with the past CERF experiments was an important achievement for the future waste characterisation. A good agreement between experimental values and predictions finally allow applying the fingerprints method to a large collection of objects which have been activated during real operation of the accelerator.

However, for a given specific activity, the contact dose-rate strongly depends on the geometry of the object. In particular, both the phenomenon of self-absorption and the non-uniform distribution of radioactive nuclides in the item of waste have an impact on the dose measurement. Depending on the prediction of the distribution and on the choice of the points to be measured, different conclusions can be drawn on the same radioactive item. It is therefore essential to test the accuracy of respective gamma spectroscopy and dose rate measurements with FLUKA predictions in a case where all these factors (shape, irradiation, material composition...) are well known.

All these ingredients finally lead to a scheme of necessary steps in order to quantify uncertainties and prove the needed accuracy of the nuclide vector approach in order to characterise the nuclear waste being produced at the CERN accelerators, especially the new LHC. As shown in Figure 11, this starts by developing a list of waste relevant materials and their detailed chemical composition based on an internal database. In addition, the list of relevant radioactive isotopes can be deducted from experience at CERN as well as taken from the experimental campaign carried out at CERF during the past years.

Figure 11: Schematic approach for the characterisation of radioactive waste in order to study the applicability of the nuclide vector approach to waste characterisation at high energy accelerators

This includes the basic requirements, the benchmark experiments as well as detailed studies of isotope production cross-sections

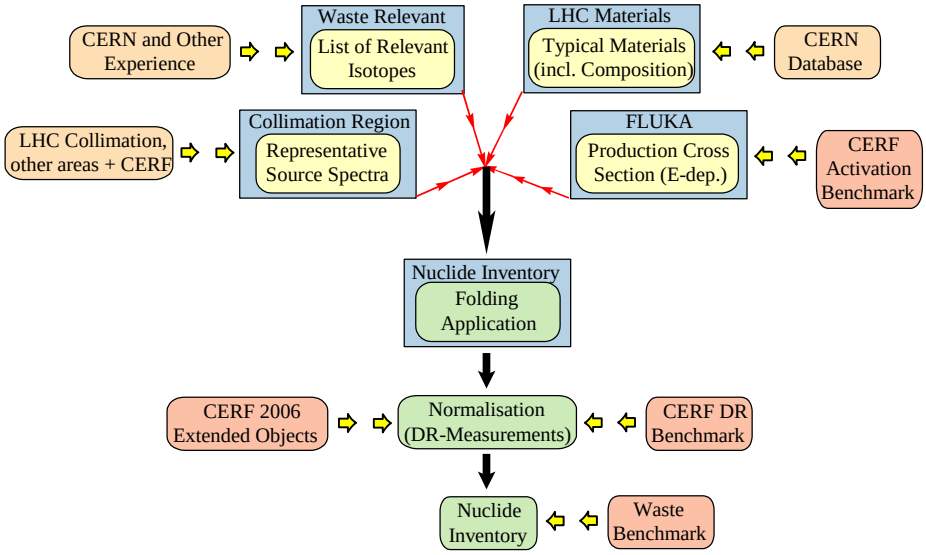

One furthermore needs a set of representative spectra being deduced by comparing spectra at all regions expected to produce radioactive waste. By folding with isotope production cross-sections and comparing the production yields for all source spectra it is possible to quantify the introduced uncertainties. Either model based (Monte Carlo, FLUKA) or evaluated experimental cross-sections can be used. The underlying uncertainties can then again be quantified by related benchmark measurements as carried out at the CERF facility or by comparing the calculated results to those available in evaluated databases.

This leads then to the definition of a possible nuclide inventory with underlying quantified uncertainties. In a next step one has to define the final normalisation of the results by either using dose rate measurements or the specific activity of representative isotopes. In order to quantify this final step leading to the definition of the nuclide inventory two additional benchmark measurements are needed. One regarding the accuracy of residual dose rates predicted with FLUKA (as successfully carried out during several benchmark experiments at CERF) and an experimental study of the influence on the agreement between measurement and simulation of residual activation when activating extended objects. The latter study includes the accuracy of mobile gamma spectrometers for so-called "fingerprint" measurements in order to determine the specific activity of representative isotopes (the latter currently being carried out at CERF).

A final step concerns the eventual application of the approach to *e.g.* the LHC in order to determine its nuclide inventory. During early operation of the LHC an accompanying experiment is needed in order to proof the above considered and quantified findings leading to the needed accuracy when predicting radioactive waste at high-energy accelerators like the CERN LHC.

Summary

All stages in the life-cycle of a high energy accelerator require calculations of induced radioactivity. For accelerators reaching TeV energies, a Monte Carlo code used for such calculations must be able to reliably predict nuclide production in interactions of all stable hadrons on arbitrary target elements and at energies ranging from that of thermal neutrons to several TeV. Most studies for the Large Hadron Collider (LHC) employ the Monte Carlo code FLUKA which was found to be the most appropriate Monte Carlo code for estimations of induced radioactivity at this accelerator as demonstrated in numerous benchmark experiments.

A general analysis of calculated isotope production cross-sections and their application to future radiation protection needs was presented. The approach showed how to quantify calculation uncertainties and use pre-calculated cross-sections in order to fold them with expected energy spectra as encountered around accelerators, thus leading to fast and accurate results.

Based on a list of materials and the produced radioactive isotopes, possible reaction channels were derived and energy-dependent isotope production cross-sections were calculated and compared to experimental data. Depending on the amount and accuracy of the available experimental data sets, as well as the production mechanisms of the radioisotopes, respective uncertainty factors were derived and quantified in a first approximation. These factors mainly depend on the production mechanism and the energy range of interest, thus allow quantifying uncertainties in isotope production as calculated with FLUKA in a more global way. It shall be noted that the latter needs a more careful analysis of the available data.

The prediction of the nuclide vector for radioactive waste considerations has been chosen as a first area of application. In particular, one of the most radioactive parts of the LHC, the collimation region, was selected. Based on an existing, detailed FLUKA geometry of that area particle fluence spectra were calculated for a large number of different locations and were folded off-line with the pre-computed cross-sections for reactions leading to waste-relevant nuclides. This approach allowed an investigation of the sensitivity of the nuclide predictions on the shape of the fluence spectra and a reduction of all computed spectra to a sub-set of so-called characteristic spectra.

The application of this approach is understood to be an indispensable ingredient, for example in order to efficiently calculate radionuclide inventories needed for disposal of radioactive waste towards the final repositories.

Acknowledgements

The authors are grateful to Alberto Fassò, Doris Forkel-Wirth and Luisa Ulrici for many stimulating discussions.

References

[1] A. Fassò, A. Ferrari, J. Ranft, P.R. Sala, *FLUKA: a Multi-Particle Transport Code*, CERN-2005-10 (2005), INFN/TC_05/11, SLAC-R-773.

[2] A. Fassò, A. Ferrari, S. Roesler, P.R. Sala, G. Battistoni, F. Cerutti, E. Gadioli, M.V. Garzelli, F. Ballarini, A. Ottolenghi, A. Empl, J. Ranft, "The Physics Models of FLUKA: Status and Recent Developments", *Computing in High Energy and Nuclear Physics 2003 Conference* (CHEP2003), La Jolla, CA, USA, 24-28 March 2003, (paper MOMT005), eConf C0303241 (2003), arXiv:hep-ph/0306267.

[3] M. Brugger, A. Ferrari, S. Roesler, L. Ulrici, "Validation of the FLUKA Monte Carlo for Predicting Induced Radioactivity at High-energy Accelerators", *Proceedings of the International Conference of the 7th International Conference on Accelerator Applications*, Venice, Italy, 2005, *Nuclear Instruments and Methods in Physics Research Section A*, Volume 562, Issue 2, pp. 814-818.

[4] Landolt-Börnstein, *Zahlenwerte und Funktionen aus Naturwissenschaften und Technik, Radionuklidproduktion bei mittleren Energien*, Bd. 13, Springer Verlag, 1991.

[5] M. Brugger, S. Roesler, L. Ulrici, "Benchmark Study of Radionuclide Production with FLUKA", *Proceedings of the Monte Carlo 2005 Conference*, Chattanooga, TN, USA, 17-21 April 2005.

[6] M. Brugger, S. Roesler, "Remanent Dose Rates Around the Collimators of the LHC Beam Cleaning Insertion", *Proceedings of the 10th International Conference on Radiation Shielding*, ICRS-10, Funchal (Madeira), Portugal, 9-14 May 2004, *Radiat. Prot. Dosim.* (2005), Vol. 115, No. 1-4, pp. 470-474.

[7] A. Mitaroff, M. Silari, "The CERN-EU High-energy Reference Field (CERF) Facility for Dosimetry at Commercial Flight Altitudes and in Space", *Radiat. Prot. Dosim.*, 102, pp. 7-22 (2002).

[8] M. Brugger, H. Khater, S. Mayer, A. Prinz, S. Roesler, L. Ulrici, H. Vincke, "Benchmark Studies of Induced Radioactivity Produced in LHC Materials, Part I: Specific Activities", *Radiation Protection Dosimetry,* 116, pp. 6-11 (2005).

[9] M. Brugger, H. Khater, S. Mayer, A. Prinz, S. Roesler, L. Ulrici, H. Vincke, "Benchmark Studies of Induced Radioactivity Produced in LHC Materials, Part II: Remanent Dose Rates", *Radiation Protection Dosimetry,* 116, pp. 12-15 (2005).

[10] A. Ferrari, *et al.*, "Nuclear Models in FLUKA: Present Capabilities, Open Problems and Future Improvements", invited talk in *Proceedings of the International Conference on Nuclear Data for Science and Technology*, Santa Fe, NM, 26 September-1 October 2004, R.C. Haight, M.B. Chadwick, T. Kawano, P. Talou (Eds.), AIP *Conference Proceedings 769*, 1197-1202 (2005).